Transaction B: Mechanical Engineering
Vol. 17, No. 1, pp. 25–40

Large Deflection of Functionally Graded Cantilever Flexible Beam with Geometric Non-Linearity: Analytical and Numerical Approaches

G.H. Rahimi[1] and A.R. Davoodinik[1,*]

Abstract. *Analytical and Adomian decomposition methods have been developed to determine the large deflection of a functionally graded cantilever beam under inclined end loading by fully accounting for geometric nonlinearities, and by incorporating the physical properties of functionally graded materials, and have also been solved. The large deflection problem will also be solved by using an FEA solver. Results obtained only due to end loading are validated using a developed analytical solution. The Adomian decomposition method yields polynomial expressions for the beam configuration. The equilibrium equation of a functionally graded cantilever beam actuated through self-balanced moments has been derived and solved using the Adomian decomposition method and the FEA solver for which no closed form solution can be obtained. Some of the limitations and recipes to obviate these are included. The Adomian decomposition method will be useful toward the design of functionally graded compliant mechanisms driven by smart actuators.*

Keywords: *Large deflection; Functionally graded flexible beams; Analytical solution; Compliant mechanism; Adomian-polynomials.*

INTRODUCTION

A compliant mechanism is a single-piece, flexible structure that delivers the desired motion and force by undergoing elastic deformation as opposed to rigid-body mechanisms. Compliant mechanisms eliminate backlash, friction and wear, and effectively reduce the production and maintenance costs associated with multiple piece assembly [1]. In such a mechanism, one or more segments is/are subjected to various types of external loading, which include actuation forces/moments and reactions from the surroundings. In the literature on compliant mechanisms, each segment is modeled as a cantilever beam [2-7]. These applications may operate under severe environmental conditions, such as high temperatures, requiring an extended operational life. Under these circumstances, the use of Functionally Graded Materials (FGM) can offer some constructive answers in order to avoid possible structural limitations. With the use of FGM, new methodologies have to be developed to design and analyze structural components made of these materials. The methods should be such that they can be incorporated into available methods with the least amount of modification, if any.

One such problem is the smart FGM compliant mechanism, i.e. one actuated by smart materials, besides external forces working at the free end of the cantilever beam (typifying the model of a compliant segment); forces and moments also exist at some intermediate locations. The self-balanced moment acting within the continuum can be interpreted as the effect of a piezo patch [8-11] perfectly bonded to the beam. Due to large deflection in the elastic region, the bending displacements can be obtained from the Euler-Bernoulli beam theory, taking into account geometric non-linearity. In the case of an isotropic compliant mechanism, the solution to the resulting non-linear differential equation has been obtained in terms of elliptic integrals of the first and second kind [12,13].

1. *Department of Mechanical Engineering, Tarbiat Modares University, Tehran, P.O. Box 14115-143, Iran.*
*. *Corresponding author. E-mail: Davoodinik@yahoo.com*

Received 24 December 2008; received in revised form 2 August 2009; accepted 27 October 2009

Such analytical solutions are possible only for uniform cross-section and simple loading conditions, like forces, at the free end. This approach has been used for developing a pseudo-rigid body model of an isotropic compliant cantilever subjected to end forces only [14]. Numerical schemes have also been proposed [15] where the forces along with moments are applied only at the free end of an isotropic compliant cantilever. The large deflection problem under combined end loadings has been solved using elliptic integrals and differential geometry in the isotropic flexural beam [16].

However, for intermediate loading, obtaining solutions using elliptic integral solutions requires a complex algorithm with an iterative procedure.

Up to now, in spite of its importance, no research work related to the smart FGM compliant mechanism has been presented.

In the present work, a study on the large deflection of a FGM cantilever beam including geometric non-linearity is performed. First, the equilibrium equation of a FGM cantilever beam for inclined end loading has been derived by fully accounting for geometric nonlinearities [17]. Then, an analytical method [13] has been developed in order to incorporate the physical properties of functionally graded materials, and solved. Secondly, the large deflection problem will also be solved by using a FEA solver such as ANSYS. For the purpose of this exercise, since the analytical solution results for the large deflection of an isotropic flexible cantilever beam are available, they will be used as verification for the ANSYS model. Next, the FGM flexible cantilever beam problem is solved by a semi-analytical method called Adomian decomposition (ADM) [18,19] for end loading and the results are compared with those obtained by using developed analytical methods and ANSYS. Finally, the equilibrium equation of a FGM cantilever beam actuated through self-balanced moments has been derived and solved using the developed ADM and FEA solver for the FGM beam.

FORMULATION OF LARGE DEFLECTION FOR CANTILEVER FGM FLEXIBLE BEAM

We model the segment of a compliant mechanism as a flexible beam with one end clamped. The dimensions in the Y- and Z-directions are represented by h and b, respectively, and are assumed to be small as compared to that in the X-direction, as shown in Figure 1, where α defines the direction of force P acting on the beam. With respect to the X-direction, ψ_0 is the slope of the reference line of the beam at end point, $C_{(x_C,y_C)}$, and ψ is the slope of the reference line of the beam at the arbitrary point, $Q_1(x_{Q1}, y_{Q1})$, of the deflected beam, with distance s from the root, both in respect to the horizontal direction.

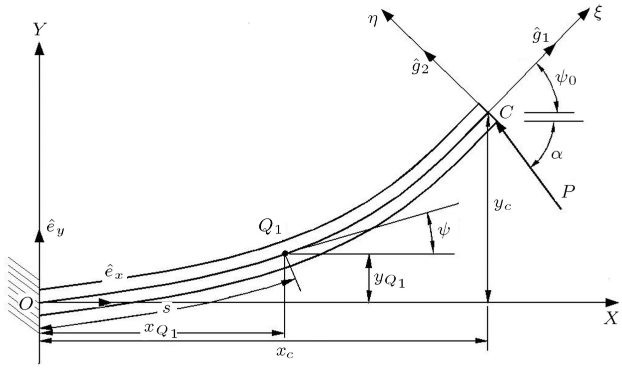

Figure 1. The cantilever flexible beam on the inclined end loading with represented Cartesian coordinate system XYZ and the orthogonal curvilinear coordinate system $\xi\eta\zeta$ for undeformed and deformed geometry, respectively.

Coordinate Transformations and Curvatures

Here, in order to derive fully nonlinear equations governing the flexible beam deformation, we introduce two coordinate systems: the inertial Cartesian coordinate system, XYZ, which describes the undeformed geometry, and the local orthogonal curvilinear coordinate system, $\xi\eta\zeta$, which describes the deformed geometry. These two coordinate systems are related by transformation matrix $[T]$ as follows:

$$\begin{Bmatrix} \hat{g}_1 \\ \hat{g}_2 \\ \hat{g}_3 \end{Bmatrix} = [T] \begin{Bmatrix} \hat{e}_x \\ \hat{e}_y \\ \hat{e}_z \end{Bmatrix},$$

$$[T] = \begin{bmatrix} \cos\psi & \sin\psi & 0 \\ -\sin\psi & \cos\psi & 0 \\ 0 & 0 & 1 \end{bmatrix}, \tag{1}$$

where $\hat{g}_j$; $(j = 1, 2, 3)$ denote the unit vectors of the system, $\xi\eta\zeta$, and $\hat{e}_x$, $\hat{e}_y$ and $\hat{e}_z$ denote the unit vectors of the system, XYZ.

Non-Linear Strain-Displacement Relations

As shown in Figure 2, according to the Euler-Bernoulli beam theory, plane sections perpendicular to the undeformed reference line remain plane and perpendicular to the deformed reference line (this is only true for thin beams). For thick beams, curvatures will not have significant changes before failure. For thin beams, curvatures may have significant changes before failure, but their shear deformations are negligible. Hence, this approximation will not cause a significant loss in accuracy [17]. To fully account for large rotations and displacements, we define displacements using a local coordinate system (s and η) to derive fully nonlinear strain-displacement relationships. To this end, first,

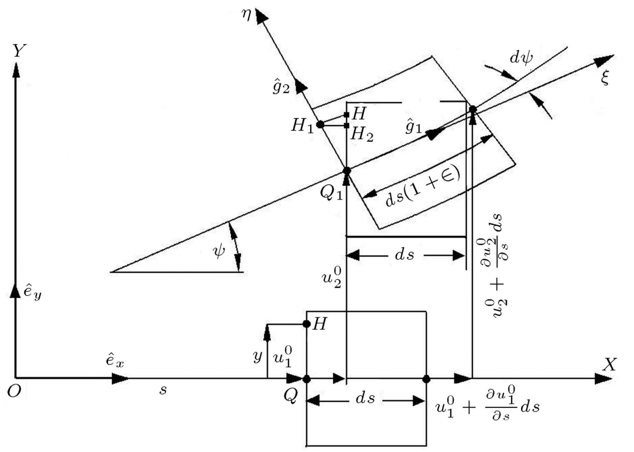

Figure 2. The observed element of flexible beam, before any deflection and after being subjected to the rigid body motion.

the global displacement field can be defined as:

$$u_1(s,y) = u_1^0(s) - y\sin\psi(s),$$

$$u_2(s,y) = u_2^0(s) - y\left[1-\cos\psi(s)\right],$$

$$u_3(s,y) = 0, \tag{2}$$

where s is the distance of the reference point (Q_1) along the length of the beam from its fixed end, u_1^0, u_2^0 are the displacements of the reference point (Q_1) on the observed element with respect to the X and Y axes, and ψ denotes the rotation angle of the observed element with respect to the $Z \equiv \zeta$ axis. Also, y is the height of any arbitrary point of cross-section H along the thickness direction, which can be presented as H_1 after beam deflection. Equations 2 are driven by the concept of infinitesimal local displacements and the following expressions:

$$QH = Q_1H_1 = y,$$

$$Q_1H_2 = y\cos\psi,$$

$$H_1H_2 = y\sin\psi,$$

$$HH_2 = y(1-\cos\psi).$$

Then, the local displacement field can be defined with respect to the deformed coordinate system (orthogonal curvilinear coordinate system, $\xi\eta\zeta$, which is co-rotated with the rigid-body motion) as:

$$\tilde{u}_1(s,\eta) = \tilde{u}_1^0(s) - \eta\sin\tilde{\psi}(s),$$

$$\tilde{u}_2(s,\eta) = \tilde{u}_2^0(s) - \eta[1-\cos\tilde{\psi}(s)],$$

$$\tilde{u}_3(s,\eta) = 0, \tag{3}$$

where, $\tilde{u}_1$, $\tilde{u}_2$ and $\tilde{u}_3$ are the local displacement components along the $\xi \equiv s$, η and $\zeta \equiv Z$ axes, respectively, and $\tilde{\psi}$ denotes the local rotation angle of the observed element.

Because the $\xi\eta\zeta$ system is a local coordinate system attached to the observed element, we have:

$$\tilde{u}_1^0 = \tilde{u}_2^0 = 0, \qquad \tilde{\psi} = \partial\tilde{u}_2^0/\partial s = 0. \tag{4}$$

Because $\tilde{u}$ is a local displacement, it is defined with respect to the deformed reference line, ξ:

$$\partial\tilde{u}_1^0/\partial s = \in, \tag{5}$$

where $\in$ is the axial strain on the deformed reference line ξ. Also, it follows from the diagram shown in Figure 3 for the infinitesimal change of a local rotation angle that:

$$\frac{\partial\tilde{\psi}}{\partial s} = \lim_{ds\to 0}\frac{d\hat{g}_1.\hat{g}_2}{ds} = \hat{g}_1'.\hat{g}_2, \tag{6}$$

where $()' = \partial()/\partial s$ and using Equations 1 and 6, we can obtain:

$$\hat{g}_1'.\hat{g}_2 = [(\cos\psi)\hat{e}_x + (\sin\psi)\hat{e}_y]'.[-(\sin\psi)\hat{e}_x + (\cos\psi)\hat{e}_y]$$

$$= -\sin\psi(\cos\psi)' + \cos\psi(\sin\psi)' = \psi' = \rho_3, \tag{7}$$

where ρ_3 is the bending curvature about the ζ axis.

Because rigid-body motions do not result in any strains or strain energy, the general form of the corresponding 2-D infinitesimal strain tensor (ε_{ij}) can be defined in terms of the local displacement vector:

$$\mathbf{U}(s,\eta) = \tilde{u}_1(s,\eta)\hat{g}_1 + \tilde{u}_2(s,\eta)\hat{g}_2, \tag{8}$$

as:

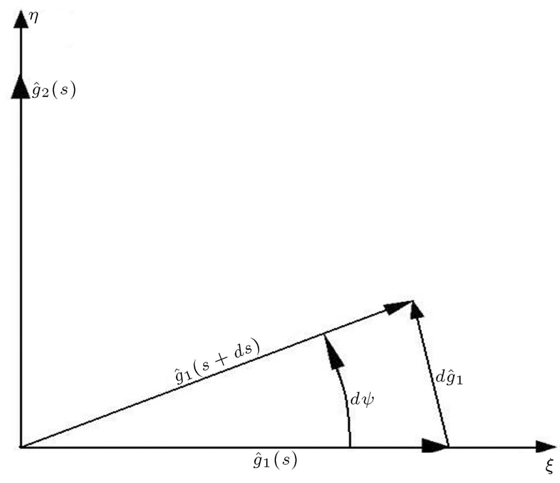

Figure 3. Concept of infinitesimal change of a local rotation angle.

$$\varepsilon_{ij} = \frac{1}{2}\left(\frac{\partial \mathbf{U}}{\partial q_i}.\hat{g}_j + \frac{\partial \mathbf{U}}{\partial q_j}.\hat{g}_i\right), \qquad i, j = 1, 2, \tag{9}$$

where $\hat{g}_1$ and $\hat{g}_2$ are unit vectors along the $q_1 \equiv \xi \equiv s$ and $q_2 \equiv \eta$ axes, respectively.

Now, by differentiating the local displacement vector, with respect to s, we have:

$$\frac{\partial \mathbf{U}}{\partial s} = \frac{\partial \tilde{u}_1}{\partial s}\hat{g}_1 + \frac{\partial \tilde{u}_2}{\partial s}\hat{g}_2 + \tilde{u}_1\frac{\partial \hat{g}_1}{\partial s} + \tilde{u}_2\frac{\partial \hat{g}_2}{\partial s}. \tag{10}$$

Then, using Equations 3 to 7 we get:

$$\partial \tilde{u}_1/\partial s = \in -\eta(\cos\tilde{\psi})\tilde{\psi}' = \in -\eta\rho_3,$$

$$\partial \tilde{u}_2/\partial s = -\eta(\sin\tilde{\psi})\tilde{\psi}' = 0. \tag{11}$$

Moreover, since $\tilde{u}_1$ and $\tilde{u}_2$ are the local displacements defined with respect to the deformed coordinate system, we have:

$$\tilde{u}_1 = \tilde{u}_2 = 0. \tag{12}$$

Thus:

$$\partial \mathbf{U}/\partial s = (\in -\eta\rho_3)\hat{g}_1. \tag{13}$$

Now, by differentiating the local displacement vector with respect to η, we have:

$$\frac{\partial \mathbf{U}}{\partial \eta} = \frac{\partial \tilde{u}_1}{\partial \eta}\hat{g}_1 + \frac{\partial \tilde{u}_2}{\partial \eta}\hat{g}_2 + \tilde{u}_1\frac{\partial \hat{g}_1}{\partial \eta} + \tilde{u}_2\frac{\partial \hat{g}_2}{\partial \eta}. \tag{14}$$

Then, using Equations 3 to 7, we get:

$$\partial \tilde{u}_1/\partial \eta = -\sin\tilde{\psi} = 0,$$

$$\partial \tilde{u}_2/\partial \eta = -(1-\cos\tilde{\psi}) = 0. \tag{15}$$

Thus:

$$\partial \mathbf{U}/\partial s = 0. \tag{16}$$

Similarly, by differentiating the local displacement vector with respect to ζ, we have:

$$\frac{\partial \mathbf{U}}{\partial \zeta} = \frac{\partial \tilde{u}_1}{\partial \zeta}\hat{g}_1 + \frac{\partial \tilde{u}_2}{\partial \zeta}\hat{g}_2 + \tilde{u}_1\frac{\partial \hat{g}_1}{\partial \zeta} + \tilde{u}_2\frac{\partial \hat{g}_2}{\partial \zeta} = 0. \tag{17}$$

Then, according to the 2-D Euler-Bernoulli beam theory, the equations describing the strains of a flexible beam are derived as:

$$\varepsilon_{11(s,\eta)} = (\partial \mathbf{U}/\partial s).\hat{g}_1 = \in -\eta\rho_3,$$

$$\varepsilon_{12} = (\partial \mathbf{U}/\partial s).\hat{g}_2 + (\partial \mathbf{U}/\partial \eta).\hat{g}_1 = 0,$$

$$\varepsilon_{22} = \varepsilon_{33} = \varepsilon_{13} = \varepsilon_{23} = 0, \tag{18}$$

where $\varepsilon_{11(s,\eta)}$ is the axial strain at any point (s, η) on the arbitrary cross-section, along the $\xi \equiv s$ axis in distance s from the fixed end. As depicted in Equation 18, according to the 2-D Euler-Bernoulli beam theory, all other components of the strain tensor are equal to zero.

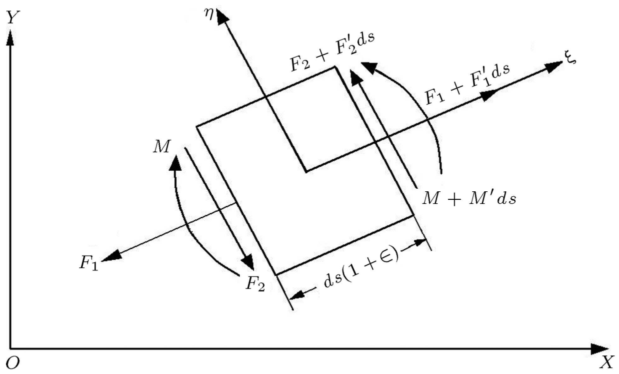

Figure 4. Free body diagram of the deflected beam element.

Equilibrium Condition of Moments

As shown in Figure 4, the equilibrium of moments, with respect to the Z direction, in any elements of the beam, by neglecting high order terms, yields:

$$M'ds + F_2(1+\in)ds = 0 \Rightarrow F_2 = -M'/(1+\in). \tag{19}$$

Moreover the equilibrium of forces in any cross-sections of the beam yields:

$$\mathbf{F} + \mathbf{P} = 0, \tag{20}$$

where $\mathbf{P}$ is the vector of end force P (Figure 1) and $\mathbf{F}$ is the resultant vector of forces on any cross-sections of the beam as:

$$\mathbf{F} = F_1\hat{g}_1 + F_2\hat{g}_2,$$

$$\mathbf{P} = (-P\cos\alpha)\hat{e}_x + (P\sin\alpha)\hat{e}_y. \tag{21}$$

Substituting Equations 1 and 21 in Equation 20 yields:

$$(-F_1\cos\psi + F_2\sin\psi)\hat{e}_x + (-F_1\sin\psi - F_2\cos\psi)\hat{e}_y$$
$$- (P\cos\alpha)\hat{e}_x + (P\sin\alpha)\hat{e}_y = 0. \tag{22}$$

Setting each of the coefficients of $\hat{e}_x$ and $\hat{e}_y$ in Equation 22 equal to zero, we obtain the equilibrium equation as:

$$-F_1\cos\psi + F_2\sin\psi - P\cos\alpha = 0, \tag{23}$$

$$-F_2\cos\psi - F_1\sin\psi + P\sin\alpha = 0. \tag{24}$$

Then, by neglecting F_1, the relation of P and F_2 can be derived as:

$$F_2 = P\sin(\alpha+\psi). \tag{25}$$

Using Equations 19 and 25, one can relate end force P and the derivative of the internal bending moment at any cross-section of the beam, M' as follows:

$$-M'/(1+\in) = P\sin(\alpha+\psi). \tag{26}$$

Material Gradient of FGM

The FGM can be produced by continuously varying the constituents of multi-phase materials in a predetermined profile. The most distinct features of an FGM are the non-uniform microstructures with continuously graded macro properties. An FGM can be defined by the variation in different manners. One such variation, which has been selected for this work, is the exponential variation (E-FGM) where the elastic module, $E_{(\eta)}$, varies according to:

$$E_{(\eta)} = E_0.e^{\lambda.\eta}, \qquad E_0 = \sqrt{E_1 E_2},$$
$$1/\lambda = h/\ln(E_2/E_1), \tag{27}$$

where h is the thickness of the beam, E_1 and E_2 are the elastic modules in $\eta = -h/2$ and $\eta = h/2$, respectively, $1/\lambda$ is *the length scale of the nonhomogeneity* and constants E_0 and $1/\lambda$ can be obtained by material gradient boundary conditions. Many researchers have found this functional form of property variation to be convenient in solving elasticity problems [20].

Stress-Strain Relationships

Because the flexible beam is a continuous system, structural or local deformations are functions of spatial coordinates. Hence, in order to state the balance of forces and moments, one can only treat an infinitesimal structural particle or element. Thus, one needs to introduce stresses and strains in order to relate the external loads to local displacements. In other words, external loads and local displacements are indirectly related in a continuous system. Since we are concerned in this paper with thin inextensible flexible beams, undergoing large global displacements and rotations but small relative displacements among points in the beam, the strain values in Equation 18 are assumed to be small and the stress-strain relations are assumed to be linear and related by a constitutive law, as:

$$\sigma_{11_{(s,\eta)}} = E_{(\eta)}\varepsilon_{11_{(s,\eta)}},$$
$$\sigma_{12} = \sigma_{22} = \sigma_{33} = \sigma_{13} = \sigma_{23} = 0, \tag{28}$$

where $\sigma_{11(s,\eta)}$ is the axial stress at any point (s,η) on the arbitrary cross-section, along the $\xi \equiv s$ axis at distance s from the fixed end. According to the 2-D Euler-Bernoulli beam theory, all other components of the stress tensor are equal to zero.

Stress Resultants and Curvatures Relations

The internal bending moment, $M \equiv M_{(s,\eta)}$, created by stress, $\sigma_{11_{(s,\eta)}}$, at any point (s,η) on the cross section of the beam at distance s from the fixed end is:

$$M_{(s,\eta)} = -\int_A \sigma_{11_{(s,\eta)}} \eta dA. \tag{29}$$

Then, considering Equations 27 to 29, we get:

$$M_{(s,\eta)} = \int_{-b/2}^{b/2}\int_{-h/2}^{h/2} E_{(\eta)}[-\eta \in +\eta^2\rho_3]d\eta dz$$
$$= E_0 \int_{-b/2}^{b/2}\int_{-h/2}^{h/2} e^{\lambda.\eta}[-\eta \in +\eta^2\rho_3]d\eta dz, \tag{30}$$

where $\lambda = 0$ (i.e. isotropic beam with the elastic module E_0), the integral in the foregoing equation is the second moment of cross-section area I_Z about the Z axis and the internal bending moment is derived the same as the Euler-Bernoulli beam theory:

$$M_{(s,\eta)_{\text{iso}}} = \int_{-b/2}^{b/2}\int_{-h/2}^{h/2} E_{(\eta)}[-\eta \in +\eta^2\rho_3]d\eta dz$$
$$= E_0\rho_3 \int_{-b/2}^{b/2}\int_{-h/2}^{h/2} [-\eta \in +\eta^2]d\eta dz$$
$$= E_0\rho_3 I_Z. \tag{31}$$

However, with $\lambda \neq 0$ (i.e. E-FGM beam), the internal bending moment for an inextensible flexible beam (i.e. $\in = 0$, where the total length of the undeformed beam is assumed to remain the same after deformation) is derived as:

$$M_{(s)} = bK_\lambda\rho_3, \tag{32}$$

where:

$$K_\lambda = (E_0/4\lambda^3 e^{\lambda h/2}) \times [e^{\lambda h}(h^2\lambda^2 - 4h\lambda + 8)$$
$$- (h^2\lambda^2 + 4h\lambda + 8)]. \tag{33}$$

Differentiating Equation 32, with respect to s, yields:

$$M'_{(s)} = bK_\lambda\rho'_3. \tag{34}$$

Using Equations 7, 26 and 34, we get:

$$bK_\lambda[d^2\psi t/ds^2] = -P\sin(\alpha+\psi). \tag{35}$$

Equation 35 is the equilibrium equation of an inextensible E-FGM flexible beam with Boundary Conditions (BCs):

$$(\psi)_{s=0} = 0,$$

and:

$$(d\psi/ds)_{s=L} = 0. \tag{36}$$

ANALYTICAL SOLUTION

In order to analytically solve Equation 35 with BCs (Equation 36), one can reduce Equation 35 to a form of Newton's equation by defining the following notations:

$$\breve{s} = s/L, \qquad \alpha_1 = \psi + \alpha, \qquad \bar{K}_\lambda = \sqrt{P/(bK_\lambda)}. \tag{37}$$

Moreover, the following derivatives can be derived:

$$\frac{d\psi}{ds} = \frac{d\alpha_1}{L.d\breve{s}} \Rightarrow \frac{d\alpha_1}{d\breve{s}} = L.\frac{d\psi}{ds}, \tag{38a}$$

$$\frac{d^2\psi}{ds^2} = \frac{d^2\alpha_1}{L^2.d\breve{s}^2} \Rightarrow \frac{d^2\alpha_1}{d\breve{s}^2} = L^2.\frac{d^2\psi}{ds^2}. \tag{38b}$$

By substituting Equations 37, 38a and 38b into Equation 35, a general non-linear second order differential equation that governs the shape of a deflected E-FGM beam is obtained as follows:

$$(d^2\alpha_1/d\breve{s}^2) + \bar{P}\sin\alpha_1 = 0, \tag{39a}$$

where $\bar{P} = (\bar{K}_\lambda L)^2$ is the normalized FGM load parameter. For given $\bar{P}$, L and λ, $\bar{K}_\lambda$can be computed and is used for obtaining numerical results.

By the way, one can convert Equation 39a for the isotropic beam such that:

$$\left(d^2\alpha_1/d\breve{s}^2\right) + \bar{P}_{\text{iso}}\sin\alpha_1 = 0, \tag{39b}$$

where $\bar{P}_{\text{iso}} = PL^2/(E_0 I_z)$ is the normalized isotropic load parameter.

To solve Equation 39a or 39b, we need two boundary conditions. Since $0 \leq s \leq L$ and $0 \leq \psi \leq \psi_0$, then from Equation 37, we can derive $0 \leq \breve{s} \leq 1$ and $\alpha \leq= \alpha_1 \leq \alpha + \psi_0$ and the boundary conditions are:

$$(\alpha_1)_{\breve{s}=0} = \alpha,$$

and:

$$(d\alpha_1/d\breve{s})_{\alpha_1=\psi_0+\alpha} = 0. \tag{40}$$

Differential Equation 39b, along with the boundary conditions given by Equation 40, has been solved by Frisch and Fay [13] for the deflected shape of a flexible isotropic beam subjected to an inclined point load at a known location. The Frisch-Fay solution describing the shape of the beam is given below:

$$x = [2\widehat{p}\sin\alpha(\cos m - \cos n) + G(\psi)\cos\alpha]/\bar{K}_\lambda, \tag{41a}$$

$$y = [2\widehat{p}\cos\alpha(\cos m - \cos n) - G(\psi)\sin\alpha]/\bar{K}_\lambda, \tag{41b}$$

where:

$$G(\psi) = [F(\widehat{p}, m) - F(\widehat{p}, n) + 2E(\widehat{p}, n) - 2E(\widehat{p}, m)], \tag{42a}$$

$$\widehat{p} = \sin[(\psi_0 + \alpha)t/2], \tag{42b}$$

$$m = \sin^{-1}[\sin(\alpha/2)/\widehat{p}], \tag{42c}$$

$$n = \sin^{-1}\{\sin[(\psi + \alpha)/2]/\widehat{p}\}. \tag{42d}$$

$\bar{K}_\lambda$ is defined in Equation 37 and $F(\widehat{p}, \Theta)$ and $E(\widehat{p}, \Theta)$, are Legendre's standard form of the first and second kinds, respectively:

$$F(\widehat{p}, \Theta) = \int_0^\Theta \frac{d\Theta}{\sqrt{1 - \widehat{p}^2 \sin^2\Theta}}, \tag{43a}$$

$$E(\widehat{p}, \Theta) = \int_0^\Theta \sqrt{1 - \widehat{p}^2 \sin^2\Theta}\, d\Theta. \tag{43b}$$

Modulus $\widehat{p}$, which governs the deflected shape of the beam, is related to the property of the beam by:

$$\bar{K}_\lambda L = [F(\widehat{p}, n) - F(\widehat{p}, m)]. \tag{44}$$

Computational Procedure

The deflected shape of the beam under a known point force (P, α) can be computed as follows:

1. For a given λ and a given force, calculate $\bar{K}_\lambda$ from Equation 37.
2. Solve for the module $\widehat{p}$ from Equation 44 implicitly. This involves constructing a function of $\widehat{p}$;

   $$f(\widehat{p}) = [F(\widehat{p}, n) - F(\widehat{p}, m)] - \bar{K}_\lambda L.$$

   Note that from the definition of $\widehat{p}$ given in Equation 42b, $0 < \widehat{p} < 1$. The equation $f(\widehat{p}) = 0$ is solved numerically, for example using the Bisection Method.
3. Calculate ψ_0 from Equation 42b.
4. Calculate m and $n_0 = n_{(\psi=\psi_0)}$ from Equations 42c and 42d, respectively.
5. Calculate the deflected shape of the beam in terms of (x and y) from Equations 41a and 41b, respectively.

ANSYS MODEL

Various finite element investigations of graded materials have been conducted using either commercially available (e.g. ABAQUS, ANSYS) or research-oriented codes. A sampling (which is by no means exhaustive) of published papers include a broad range of applications, such as elasticity [21,22] and functionally graded piezoelectric actuators [23,24].

Modeling of FGMs by the FEM can be accomplished by using either graded or homogeneous elements [21,22]. Figure 5a shows an example of an exponentially graded material and Figure 5b illustrates a domain made of this material. The graded element (see Figure 5c) incorporates the material property gradient at the size scale of the element, while the homogeneous element (see Figure 5d) produces a stepwise constant approximation to a continuous material property field. The symbol "*o*" in Figure 5c indicates the location for material property sampling.

Characteristics of Selected Element

The ANSYS model was built using a Solid Shell 190 element, which is a newer hybrid type element that builds and meshes like a brick element, but allows for layered material properties like a shell element. This element has large deflection (non-linear geometry) capability. The Solid Shell element is potentially very suitable for modeling a functionally graded material.

A Solid Shell 190 is an eight-node solid element that has hybrid capabilities, like both a shell and a solid element. The benefit is that the element can provide the layering properties of a shell and accommodate varying material properties through the element thickness, but can be built and viewed as a brick. The Solid Shell 190 element would have been ideal for performing a strictly structural analysis.

The ANSYS code was used to create a change in the material properties of the meshed elements through the thickness of the material in order to create the effects of the functionally graded flexible beam. The tricky part of the coding was handling the functionally graded material. The beam was first created and meshed into multiple layers with all of one material type. Then, a *do loop* was written into the code to grade the material properties through the thickness. The code was written robustly enough so that the number of line divisions could be altered without affecting the material properties of the elements in each layer.

If the validity of the isotropic material model were verified, a solution for the functionally graded material model could be attempted.

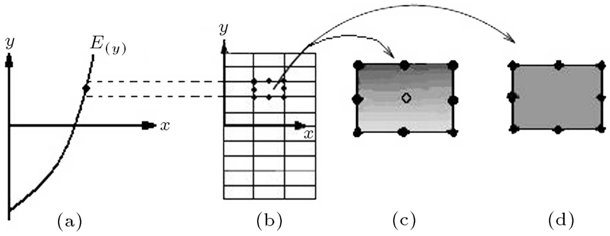

Figure 5. FEM modeling of E-FGM: (a) Nonhomogeneous medium; (b) Generic region; (c) Graded element; (d) Homogeneous element.

DECOMPOSITION METHOD

Recently, a great deal of interest has been focused on the application of Adomian's decomposition method for the solution of boundary value problems [25,26] or for verification of results obtained by their new methods [27]. Here, the decomposition method is discussed in a nutshell.

We consider an equation in the form $Lu + Ru + Nu = g$, where L is an easily or trivially invertible linear operator, R is the remaining linear part, N represents a nonlinear operator, and g is known. The general solution of the given equation is decomposed into the sum, $u = \sum_{n=0}^{\infty} u_n$, where u_0 is the solution of the linear part. Our approach will be to write any nonlinear term in terms of the Adomian A_n polynomials. It has been derived by Adomian that $Nu = \sum_{n=0}^{\infty} A_n(u_0, u_1, u_2, u_3, \cdots, u_n)$, where the A_n are special polynomials obtained for particular nonlinearity $Nu = f(u)$ and generated by Adomian [18,28,29]. These A_n polynomials depend, of course, on the particular nonlinearity. The A_n are given as:

$$A_0 = f(u_0),$$

$$A_1 = u_1 \left(\frac{d}{du_0}\right) f(u_0),$$

$$A_2 = u_2 \left(\frac{d}{du_0}\right) f(u_0) + \left(\frac{u_1^2}{2!}\right)\left(\frac{d^2}{du_0^2}\right) f(u_0),$$

$$A_3 = u_3 \left(\frac{d}{du_0}\right) f(u_0) + u_1 u_2 \left(\frac{d^2}{du_0^2}\right) f(u_0) + \left(\frac{u_1^3}{3!}\right)\left(\frac{d^3}{du_0^3}\right) f(u_0),$$

$$\vdots$$

and can be found from the formula (for $n \geq 0$):

$$A_n = \frac{1}{n!}\frac{d^n}{d\Omega^n}\left[N\left[\sum\nolimits_{k=0}^{\infty} \Omega^k u_k\right]\right]_{\Omega=0}. \tag{45}$$

Therefore, the general solution becomes:

$$u = u_0 - L^{-1}R\sum_{n=0}^{\infty} u_n - L^{-1}Nu$$

$$= u_0 - L^{-1}R\sum_{n=0}^{\infty} u_n - L^{-1}\sum_{n=0}^{\infty} A_n, \qquad (46)$$

where:

$$u_0 = \phi + L^{-1}g,$$

and:

$$L\phi = 0.$$

If $L \equiv d^n/dt^n$ with t as an independent variable, then L^{-1} is the n-fold definite integral with respect to t, with limits from 0 to t. Thus, if we have a second order linear operator, Equation 46 yields:

$$u = u(0) + u'(0)t + L^{-1}g - L^{-1}R\sum_{n=0}^{\infty} u_n$$

$$- L^{-1}\sum_{n=0}^{\infty} A_n, \qquad (47)$$

or an IVP, $u(0)$ and $u'(0)$ are specified. On the other hand, for a BVP, $u(0)$ is specified but $u'(0)$ is to be determined by satisfying the second boundary condition of $u(t)$. Now, $u_0 = u(0) + u'(0)t + L^{-1}g$ and the solution is obtained as $u = u_0 + \sum_{n=1}^{\infty} u_n$. To identify the terms in $\sum_{n=1}^{\infty} u_n$, it has been derived by Adomian that:

$$u_{n+1} = -L^{-1}Ru_n - L^{-1}A_n, \qquad n \geq 0. \qquad (48)$$

From Equation 48, we can write $u_1 = -L^{-1}Ru_0 - L^{-1}A_0$, thus u_1 can be calculated in terms of the known u_0. Now:

$$u_2 = -L^{-1}Ru_1 - L^{-1}A_1,$$

$$u_3 = -L^{-1}Ru_2 - L^{-1}A_2, \qquad (49)$$

and so on.

Hence, all the terms of u are now calculated and the general solution is obtained as:

$$u = \sum_{n=0}^{\infty} u_n. \qquad (50)$$

Recently, the Adomian decomposition method was reviewed and a mathematical model of Adomian polynomials was introduced in [30]. The resulted solution converges [31] to the closed form solution if an exact solution exists for the equation.

SOLVING FGM BEAM PROBLEM USING ADOMIAN DECOMPOSITION

Integrating Equation 36 twice, with respect to s one gets:

$$\psi(s) = \psi(0) + \left.\frac{d\psi}{ds}\right|_{s=0} s + \int_0^s \int_0^t N(\psi)dsdt, \qquad (51)$$

where:

$$N(\psi) = -(P/bK_\lambda)(\sin\alpha\cos\psi + \cos\alpha\sin\psi). \qquad (52)$$

Applying the BCs described in Equation 36 and assuming $d\psi/ds|_{s=0} = c$, Equation 51 yields:

$$\psi(s) = cs + \int_0^s \int_0^t N(\psi)dsdt. \qquad (53)$$

Now, using Equations 45, 48 and 53, from which c is determined, and satisfying the BC $d\psi/ds|_{s=L} = 0$, all ψ_n's can be calculated. Thus, the solution can be written as:

$$\psi(s) = \sum_{n=0}^{m} \psi_n, \qquad (54)$$

where the $(m+1)$th term onwards will have an insignificant contribution. Once $\psi(s)$ is known, the coordinates of any point on the beam, $(x(s), y(s))$, can be obtained by using $dx/ds = \cos\psi$ and $dy/ds = \sin\psi$.

The expressions for $\psi(s)$ as a function of c, α and $\bar{K}_\lambda$ are computed, considering up to the 8th term of the Adomian polynomials; the details are given in Appendix A.

CANTILEVER BEAM UNDER SELF-BALANCED MOMENT AND EXTERNAL LOAD

The effect of a pair of piezo patches, mounted on two opposite sides of a cantilever beam driven out of phase, is modeled [8-11] as two concentrated self-balanced moments acting at the edge of the piezo patches (Figure 6). The magnitude of the moments depends on the applied voltage across the piezo and its material properties. In this section, a large deflection cantilever beam has been modeled under self-balanced moments as well as external force, at the free end and solved using the Adomian decomposition method.

Adomian Decomposition Method

While using the Adomian decomposition method, first the cantilever beam is discretized into three segments, as shown in Figure 7, so that the self-balanced moments (M_1) are acting just on the end points of the intermediate section. Thus, the length of the intermediate segment is the same as that of the piezo actuator,

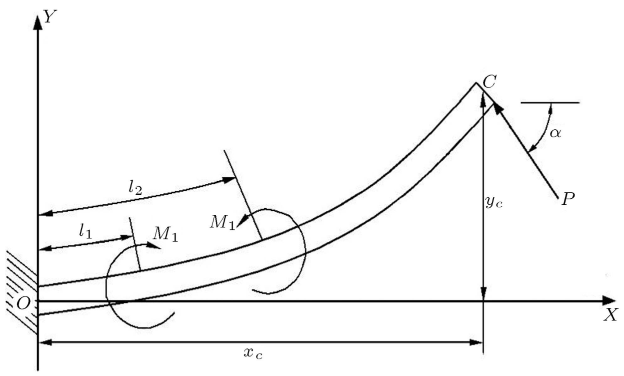

Figure 6. Cantilever beam subjected to self-balanced moment and end load.

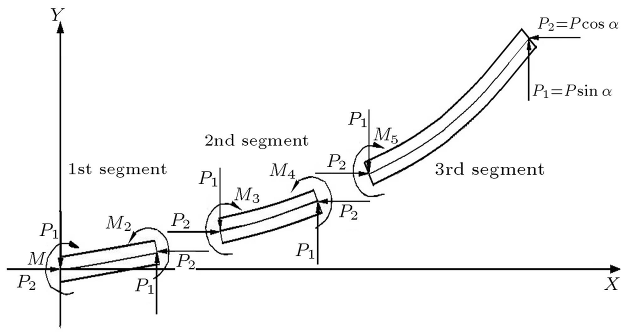

Figure 7. The free body diagram of the three segments of the cantilever beam.

i.e. $(l_2 - l_1)$ and the first and last segments are of length l_1 and $(L - l_2)$, where L is the length of the entire beam. The external forces in each of the segments are clearly depicted in Figure 7. Each of the segments is considered as a beam undergoing large deformation, for which the governing equation is solved using the Adomian decomposition method. The force and moment equilibrium and the continuity of the displacement and slope are maintained at every junction.

The actuating moment, M_1, can be normalized as $\bar{M} = (m_1 L)/(bK_\lambda)$.

Segmentation of the Beam

Considering any segment as a cantilever beam shown in Figure 7, the governing equation is obtained from Equations 51 and 52 for any segment as:

$$\psi_i(s_i) = \psi_i(0) + \left.\frac{d\psi_i}{ds_i}\right|_{s_i=0} s_i - \left(\frac{P}{bK_\lambda}\right)\int_0^{s_i}\int_0^{t}(\sin\alpha\cos\psi_i + \cos\alpha\sin\psi_i)ds_i dt, \tag{55}$$

where $i = 1, 2, 3$ and $\psi_i(s_i)$ is the slope at any point on the ith segment at distance s_i from the left end of the ith segment along its length in the beam. The BCs are:

$$(\psi_1)_{s_1=0} = 0, \qquad (d\psi_1/ds_1)_{s_1=0} = c, \tag{56}$$

and:

$$(\psi_2)_{s_2=0} = (\psi_1)_{s_1=l_1},$$

$$\left.\frac{d\psi_2}{ds_2}\right|_{s_2=0} = \frac{M_3}{K_\lambda b} = \left.\frac{d\psi_1}{ds_1}\right|_{s_1=l_1} + \frac{M_1}{K_\lambda b}, \tag{57}$$

and:

$$(\psi_3)_{s_3=0} = (\psi_2)_{s_2=l_2-l_1},$$

$$\left.\frac{d\psi_3}{ds_3}\right|_{s_3=0} = \frac{M_5}{K_\lambda b} = \left.\frac{d\psi_2}{ds_2}\right|_{s_2=l_2-l_1} - \frac{M_1}{K_\lambda b}, \tag{58}$$

for the first, second and third segment of the beam, respectively, where c is the unknown to be determined. The non-linear term of Equation 55 can be expressed in terms of Adomian polynomials. Solution $\psi_1(s_1)$ can be determined as a polynomial of s_1 and c, the solution $\psi_2(s_2)$ as a polynomial of s_1, s_2, c and M_1, and finally solution $\psi_3(s_3)$ as a polynomial of s_1, s_2, s_3, c and M_1 using the decomposition method as illustrated previously.

Thus, $\psi_{(s)}$, the slope at any point on the entire beam, is known in terms of c and M_1. Now, c should be such that $(d\psi_3/ds_3)$ at the end of the beam (i.e. $s_3 = L$) is equal to zero. Using this BC, c is determined and thus $\psi_{(s)}$ can be calculated at any point of the beam as a function of M_1, i.e. the actuating self-balancing moments. Once $\psi_{(s)}$ is known, $(x(s), y(s))$ are obtained using $dx/ds = \cos\psi$ and $dy/ds = \sin\psi$.

RESULTS AND DISCUSSION

As mentioned previously, if the validity of the ANSYS model for isotropic material were verified, the solution for the functionally graded material model could be attempted.

First, in order to show the accuracy of the ANSYS model, the convergence table with the results for the large deflection of an isotropic flexible cantilever beam due to end loading (with condition $\bar{P}_{\text{iso}} = 0.2$ and $\alpha = \pi/2$) is shown in Table 1. The directions of forces, as shown in Figure 1, are assumed to be positive. The non-dimensional end point co-ordinate ($\bar{x} = x_C/L$, $\bar{y} = y_C/L$) obtained by the ANSYS model and that of the analytical solution (elliptic integral solution) are furnished in Table 1. The computational procedure (explained in previous sections) is used in the elliptic integral solution to derive the coordinates of the deflected beam.

In the ANSYS model, a fine mesh needs to be developed in order to get an accurate result for the

Table 1. The convergence table with the results for the large deflection of isotropic and FGM flexible cantilever beam due to the end loading.

Number of SOLSH190 Elements per inch	Loading Condition	End Point Co-Ordinate			
		$\bar{x}$	Percent Error	$\bar{y}$	Percent Error
20	$\bar{P}_{\text{iso}} = 0.2$, $\alpha = \pi/2$	0.997460000	0.01%	0.064877333	-2.24%
	$\bar{P} = 0.75$, $\alpha = \pi/2$	0.967425333	0.15%	0.230486666	-2.17%
40	$\bar{P}_{\text{iso}} = 0.2$, $\alpha = \pi/2$	0.997455200	0.01%	0.064944000	-2.14%
	$\bar{P} = 0.75$, $\alpha = \pi/2$	0.967406666	0.14%	0.230566666	-2.14%
80	$\bar{P}_{\text{iso}} = 0.2$, $\alpha = \pi/2$	0.997453933	0.01%	0.064961333	-2.12%
	$\bar{P} = 0.75$, $\alpha = \pi/2$	0.967398666	0.14%	0.230600000	-2.13%
120	$\bar{P}_{\text{iso}} = 0.2$, $\alpha = \pi/2$	0.997453733	0.01%	0.064964333	-2.11%
	$\bar{P} = 0.75$, $\alpha = \pi/2$	0.967396666	0.14%	0.230606666	-2.12%

deflection problem. When the resolution is at 120 elements per inch through the length of the beam, the deflection converges to less than 2.5% error, when compared to the analytical solution. The converged mesh was one element thick through the thickness of the beam, which is fine for an isotropic problem, but which will have to be changed up to 500 elements per inch for functionally graded material properties which need multiple layers through the thickness of the beam. Interestingly enough, it can be investigated that the ANSYS model convergence with the Solid Shell 190 element not only was reached quicker than that of any brick elements, but was also computationally more effective than any of the brick elements.

The deformed configuration of the isotropic cantilever beam due to the end loading computed using the ADM and ANSYS model and elliptic integral solutions, are shown in Figure 8. Each point (x, y) on the beam is normalized as $(x/L,\ y/L)$ where L is the length of the unstretched beam. Three cases are considered for comparison: Case I ($\bar{P}_{\text{iso}} = 1.3072$, $\alpha = \pi/2$), Case II ($\bar{P}_{\text{iso}} = 0.9$, $\alpha = \pi/2$) and Case III ($\bar{P}_{\text{iso}} = 0.2$, $\alpha = \pi/2$). It can be seen that for low values of the isotropic load parameter (i.e., say up to $\bar{P}_{\text{iso}} \leq 0.2$), the ANSYS model is reliable. However, for $\bar{P}_{\text{iso}} > 0.2$, the difference starts to become significant and the higher the value of $\bar{P}_{\text{iso}}$, the larger the deviation. The experimental result that is available for Case I [17] is also presented in Figure 8.

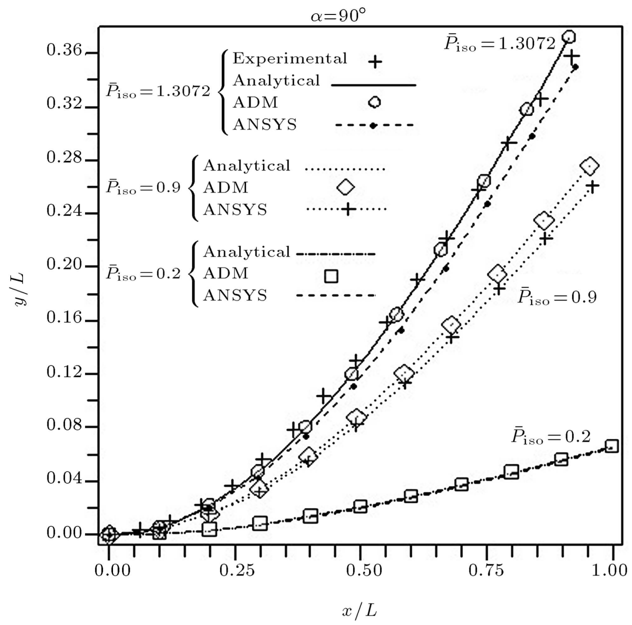

Figure 8. Isotropic beam configuration obtained under end force ($\alpha = \pi/2$).

Now, in order to evaluate the accuracy of the ANSYS model and the ADM solutions for a FGM flexible cantilever beam, the deformed configuration of the FGM beam due to the end loading computed using the ADM and the ANSYS model and elliptic integral solutions, are shown in Figure 9. Three cases are considered for comparison; Case IV ($\bar{P} = 3$, $\alpha = \pi/4$), Case V ($\bar{P} = 1$, $\alpha = \pi/4$) and Case VI ($\bar{P} = 0.75$, $\alpha = \pi/4$). It can be seen that ANSYS model results are reliable for values of a FGM load parameter up to $\bar{P} \leq 0.75$. In order to show the accuracy of the ANSYS model, the convergence results for the large deflection of a FGM flexible cantilever beam due to end loading with condition $\bar{P} = 0.75$, $\alpha = \pi/2$ are also presented in Table 1.

The solutions obtained from the ADM and ANSYS model have been compared numerically with the existing elliptic integral solutions and are presented in Table 2.

The ADM results are obtained using up to the 8th term of the Adomian polynomials. The ADM results are obtained with a tolerance level for error in the curvature as 10^{-7}. These are seen to be accurate up to four decimal places and further accuracy can be achieved by decreasing the allowable tolerance.

Using ADM and the same number of terms in

Table 2. Comparison of numerical accuracy of the solutions obtained from elliptic integral, Adomian decomposition method and ANSYS model.

Loading Condition	**End Point Coordinate, Analytical Solution**		**End Point Coordinate, ADM (up to 8th Order Terms)**		**End Point Coordinate, ANSYS Model**	
	$\bar{x}$	$\bar{y}$	$\bar{x}$	$\bar{y}$	$\bar{x}$	$\bar{y}$
$\bar{P}=3$, $\alpha=\pi/4$	0.557202013	0.732975660	0.557383268	0.732965095	0.586540000	0.716453333
$\bar{P}=1$, $\alpha=\pi/4$	0.945496556	0.295576844	0.945494262	0.295574167	0.949346000	0.284920000
$\bar{P}=0.75$, $\alpha=\pi/4$	0.972162061	0.213078291	0.972169927	0.213075856	0.973233333	0.208733333
$\bar{P}=0.75$, $\alpha=\pi/2$	0.966026250	0.235622029	0.966033707	0.235615159	0.967396666	0.230606666

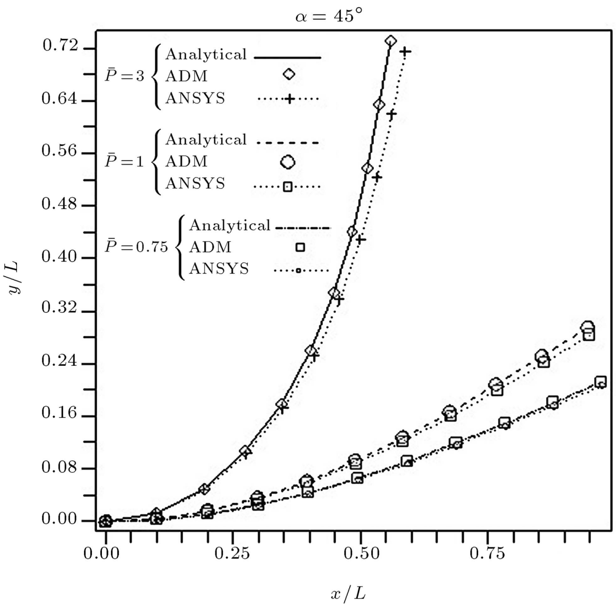

Figure 9. FGM beam configuration obtained under inclined end force.

Adomian polynomials and the same tolerance used in isotropic beams, the deflected FGM beam shape shows very little discrepancy from the analytical solution up to $\bar{P}=3$. The convergence of the ADM for the FGM flexible beam problem is demonstrated in Table 3.

Here, the coordinates of the end point of the beam are computed for an increasing number of terms in the Adomian polynomial. It is seen that inclusion up to the 8th term in the Adomian polynomial is sufficient.

The disadvantage of the ANSYS model, even for values of FGM load parameter up to $\bar{P} \leq 0.75$, is the large deviation of the ANSYS model results from the ADM and analytical results when the variation of the FGM load parameter is only obtained by variation of the power law exponent (λ). This is not improved by increasing the number of elements through the thickness of the FGM beam. In order to show this discrepancy, the deformed configuration of the FGM cantilever beam due to end loading computed using the ANSYS model, the ADM and elliptic integral solutions, is shown in Figure 10. Two cases are considered for comparison: Case VII ($\bar{P}=0.75$, $\alpha=\pi/4$,) and Case IIX ($\bar{P}=0.3006$, $\alpha=\pi/4$) obtained by the substitution of λ with $\vartheta\lambda$ in Case VII (all other parameters in $\bar{P}=(\bar{K}_\lambda L)^2$ are constant). It can be seen that ANSYS model results are not reliable for Case IIX.

The advantage of the Adomian decomposition method is that once the closed form expression is obtained, it can be used for various values of FGM loading parameters without recalling the program each time. However, with increasing load, more terms in the

Table 3. Proof of convergence of Adomian decomposition method.

Number of Terms in Adomian Polynomial	**End Point Coordinate for $\bar{P}=1$, $\alpha=\pi/4$**		
	$\bar{x}$	$\bar{y}$	c
1	0.966930294	0.232352047	0.047140452
2	0.931082426	0.330118244	0.064328431
3	0.946282992	0.293577801	0.058207421
4	0.945575475	0.295364769	0.058469208
5	0.945397001	0.295820710	0.058542814
6	0.945518630	0.295512534	0.058495142
7	0.945490989	0.295582421	0.058505814
8	0.945494262	0.295574167	0.058504570
9	0.945494262	0.295574167	0.058504570

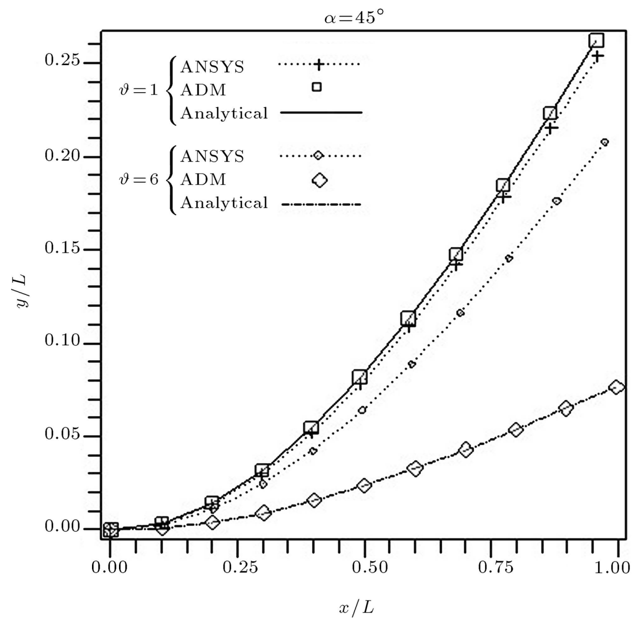

Figure 10. FGM beam configuration obtained under inclined end force when the variation of FGM load parameter is only obtained by the variation of the power law exponent (λ).

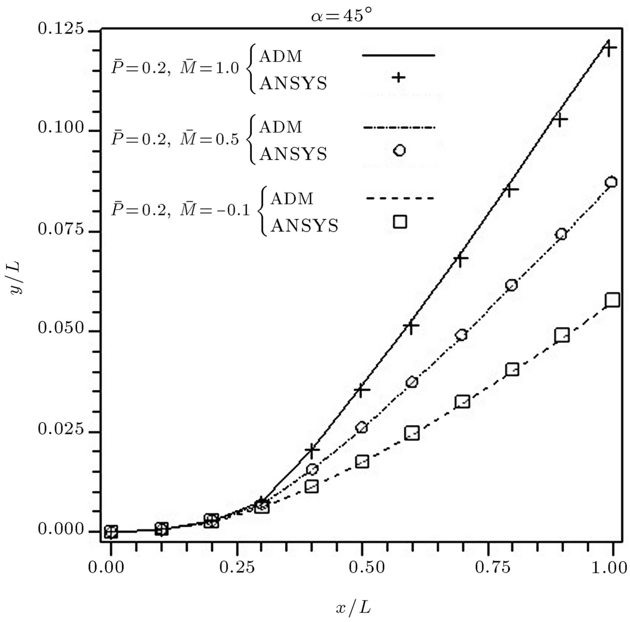

Figure 11. FGM beam configuration due to various values of the positive self-balanced moment and a constant inclined end force ($\bar{P} = 0.2$, $\alpha = \pi/4$).

polynomial need to be retained for the same level of accuracy. In this method, the unknown $d\psi/ds|_{s=0} = c$ is determined satisfying the second boundary condition given in Equation 36. Satisfying the moment boundary condition specified at the free end, higher order polynomials in 'c' are obtained, hence multiple solutions are obvious. Depending on each and every real value of 'c', a beam configuration can be obtained for the zero bending moment (curvature) at the fixed end, which can also be developed for problems with a non-zero bending moment at the free end. If the calculated value of the curvature at $s = 0$ matches the value of c, then the solution corresponding to that particular c is valid. Using this algorithm, only one valid beam configuration has been obtained.

The Adomian decomposition method can be used to determine the deformed FGM beam shape under self-balanced moment and external load as well. Figures 11, 12 and 13 show the deformed beam configuration obtained by using ADM and the ANSYS model. In each case, actuating moments are assumed to be acting at $l_1/L = 0.25$ and $l_2/L = 0.35$, which implies that the length of the piezoelectric element, i.e. $(l_2 - l_1)$, is 10% of the length of the beam. Figures 11 and 12 are obtained for a constant inclined end force ($\bar{P} = 0.2$, $\alpha = \pi/4$) and various values of the positive and negative actuating moments, respectively, while Figure 13 is obtained for a constant negative actuating moment and various values of the inclined end forces with $\alpha = \pi/4$.

It can be observed that each of the cases in Figures 12 and 13 incorporates an inflection point (a point where the moment is zero). For low values of FGM load parameters, both methods (ANSYS model and Adomian decomposition method) yield almost the same configuration. But, by increasing load parameters, there is a significant discrepancy between the two results.

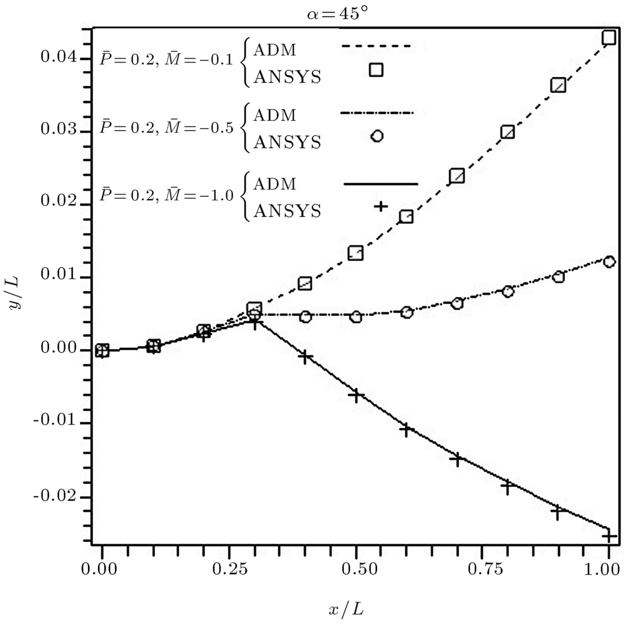

Figure 12. FGM beam configuration due to various values of the negative self-balanced moment and a constant inclined end force.

As presented in Figure 14, the inflection points can be obtained by calculation of the variations of the slope of the deflected beam (i.e. $d\psi/ds$) along the non-

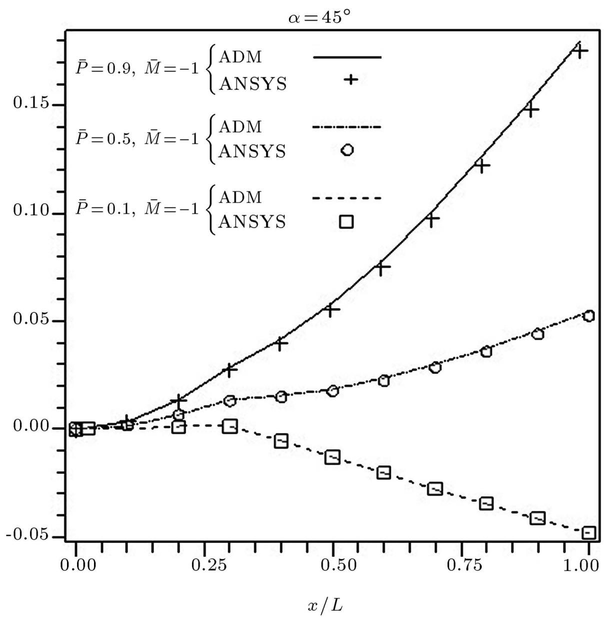

Figure 13. FGM beam configuration due to various values inclined end force and the constant negative self-balanced moment.

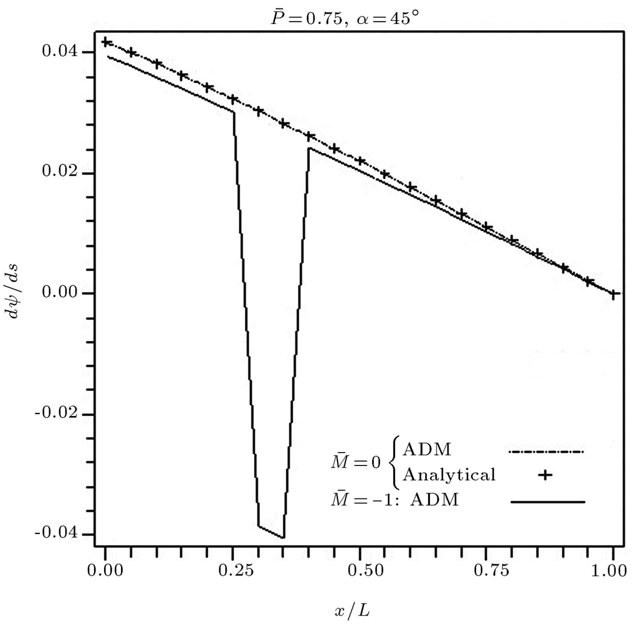

Figure 14. The variations of the slope of the deflected beam (i.e. $d\psi/ds$) along the non-dimensional length of the beam (x/L).

dimensional length of the beam (x/L).

The Adomian decomposition method can be used to determine the effect of the variation of the power law exponent (λ) on the deformed FGM beam shape. As mentioned in Equation 27, this variation can be presented as the ratio of the modulus of elasticity (i.e. $\bar{E} = E_2/E_1$ where E_2 and E_1 were defined previously). Figure 15 shows the deflection of the FGM beam with different $\bar{E}$ due to vertical end loading (i.e. $\alpha = \pi/2$). Three values of $\bar{E}$ (i.e. $\bar{E} = 1,\ 5,\ 10$) are considered ($\bar{E} = 1$ for the isotropic beam). As shown in Figure 15, while all other parameters are constant, increasing $\bar{E}$ can yield to the decreasing of the slope of any point of the deflected beam.

Figure 16 shows the deflection of the FGM beam due to different end loading angles. Four values of end loading angle (i.e. $\alpha = \pi/2,\ \pi/3,\ \pi/4$ and $\pi/6$) for selected values of the FGM load parameter and actuating moment (i.e. $\bar{P} = 0.75$ and $\bar{M} = -1$) are

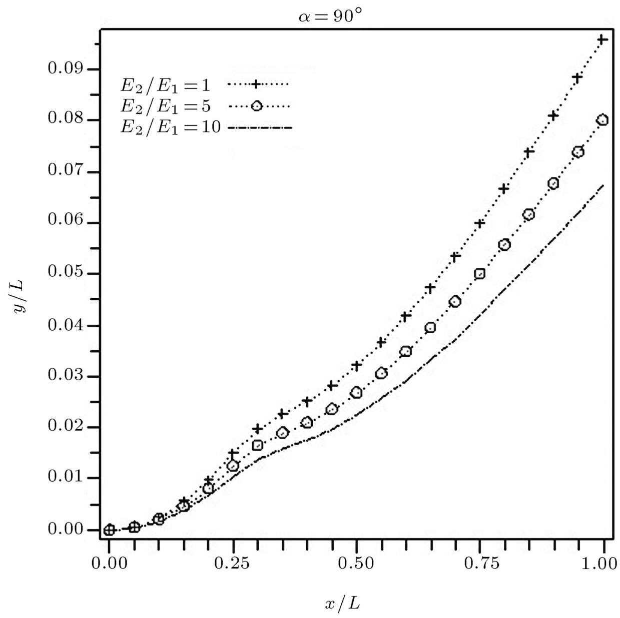

Figure 15. The deflection of the FGM beam with different $\bar{E} = E_2/E_1$ due to constant negative internal moments and vertical end loading.

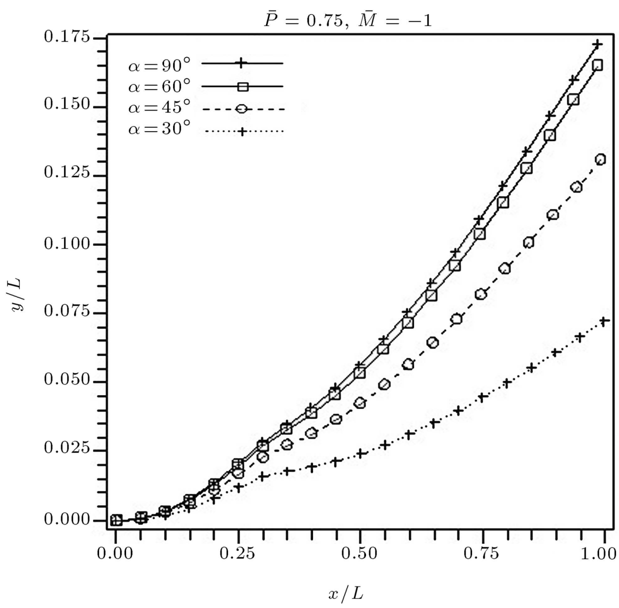

Figure 16. The deflection of the FGM beam due to different end loading angles.

considered. As shown, by increasing the end loading angle, the slope of any point of the deflected beam is increased.

On the whole, all these results reveal that the analytical solution that has been developed for a FGM cantilever flexible beam is very accurate and can be used for inclined end force loading conditions, independently of the values of FGM loading parameters. The ANSYS model can also be used for a FGM flexible beam, but the maximum values of FGM loading parameters are limited. For the Adomian decomposition method, the limitation of maximum values of FGM loading parameters is larger than the ANSYS model. Moreover, when the variation of the FGM load parameter is only obtained by the variation of the power law exponent (λ), the deformed configuration of the FGM cantilever beam due to end loading computed, using the ANSYS model, has a large discrepancy with analytical results. While, when the variation of the FGM load parameter is only obtained by variation of the power law exponent (λ), the deformed configuration of the FGM cantilever beam due to end loading computed, using ADM, matches pretty well with analytical results.

Furthermore, for the Adomian decomposition method, once the closed form expression is obtained, it can be used for various values of loading parameter. However, in the Adomian method, the higher the number of discrete loadings, the larger the number of segments to be considered (as discussed in previous sections), thus the computational complexity increases. Overall, this method can be used to solve the large deflection problem of a FGM beam, considering geometric non-linearity under any type of static loading for which no comfortable closed form solution is possible.

CONCLUSION

An analytical method has been developed in order to incorporate the physical properties of functionally graded materials for a FGM cantilever flexible beam, and then solved for inclined end loading conditions. The FGM large deflection problem has also been solved using the ANSYS model. For the purpose of this exercise, the ANSYS code was used to create a change in the material properties of meshed elements through the thickness of the material in order to create the effects of a functionally graded flexible beam. Then, analytical solution results for the large deflection of a FGM flexible cantilever beam have been used as verification for the ANSYS model. Next, the FGM flexible cantilever beam problem is solved by a semi-analytical method, called Adomian decomposition, for end loading, and validated against analytical methods, while determining large deflection under inclined end loading conditions. The semi-analytical method and the ANSYS model can handle static, concentrated and/or discretely distributed loadings. It is observed that these methods are totally insensitive to the existence of any inflection point. The Adomian decomposition procedure is envisaged as being useful for modeling the actuation of smart FGM compliant mechanisms by discretely distributed smart actuators. In future, this solution procedure will be extended to analyze FGM beams with an arbitrary variation of geometry (for which a closed form solution is impossible).

REFERENCES

1. Ananthasuresh, G.K. and Kota, S. "Designing compliant mechanisms", *Mechanical Engineering*, pp. 93-96 (November 1995).
2. Korayem, M.H. et al. "The effect of payload variation on the residual vibration of flexible manipulators at the end of the given path", *Scientia Iranica, Trans. B*, **16**(4) pp. 332-343 (2009).
3. Zohoor, H. and Khorsandijou, S.M. "Dynamic model of a mobile robot with long spatially flexible links", *Scientia Iranica, Trans. B*, **16**(5), pp. 387-412 (2009)
4. Pourtakdoust, S.H. and Assadian, N. "Aeroelastic analysis of guided hypersonic launch vehicles", *Scientia Iranica*, **11**(1,2), pp. 26-36 (April 2004).
5. Vossoughi, G.R. and Karimzadeh, A. "Impedance control of a flexible link robot for constrained and unconstrained maneuvers using sliding mode control (SMC) method", *Scientia Iranica*, **14**(1), pp. 33-45 (February 2007).
6. Gharesi Fard, B. et al. "Multi-input multi-output direct adaptive control for a distributed parameter flexible rotating arm", *Scientia Iranica*, **15**(1), pp. 65-74 (February 2008).
7. Korayem, M.H. and Nikoobin, A. "Formulation and numerical solution of robot manipulators in point-to-point motion with maximum load carrying capacity", *Scientia Iranica, Transaction B*, **16**(1), pp. 101-109 (February 2009).
8. Crawley, E.F. and Luis, J. "Use of piezoelectric actuators as elements of intelligent structures", *AIAA J.*, **25**, pp. 1373-1385 (1987).
9. Crawley, E.F. "Intelligent structures for aerospace: a technology overview and assessment", *AIAA J.*, **32**, pp. 1689-1699 (1994).
10. Wang, B.T. and Rogers, C.A. "Modeling of finite length spatially-distributed induced strain actuators for laminate beams and plates", *J. Intell. Mater. Syst. Struct.*, **2**, pp. 38-58 (1991).
11. Gaudenzi, P. and Barboni, R. "Static adjustment of beam deflections by means of induced strain actuators", *Smart Mater. Struct.*, **8**, pp. 278-283 (1999).
12. Bisshop, K.E. and Drucker, D.C. "Large deflection cantilever beams", *Q. Appl. Math.*, **3**, pp. 272-275 (1945).

13. Frisch-Fay, R., *Flexible Bars*, Washington, Butterworths (1962).
14. Howell, L.L. and Midha, A. "Parametric deflection approximations for end loaded large deflection beams in compliant mechanisms", *ASME J. Mech. Des.*, **117**, pp. 156-165 (1995).
15. Saxena, A. and Kramer, S.N. "A simple and accurate method for determining large deflections in compliant mechanisms subjected to end forces and moments", *ASME J. Mech. Des.*, **120**, pp. 392-400 (1998).
16. Kimball, C. and Tsai, L.W. "Modeling of flexural beams subjected to arbitrary end loads", *ASME J. Mech. Des.*, **124**, pp. 223-234 (2002).
17. Frank, P.P. et al. "Large-deformation tests and total-Lagrangian finite-element analyses of flexible beams", *International Journal of Solids and Structures*, **37**, pp. 2951-2980 (2000).
18. Adomian, G., *Solving Frontier Problems of Physics: The Decomposition Method*, Kluwer, Boston (1994).
19. Banerjee, A. et al. "Large deflection of cantilever beams with geometric non-linearity: Analytical and numerical approaches", *International Journal of Non-Linear Mechanics*, **43**, pp. 366-376 (2008).
20. Suresh, S. and Mortensen, A., *Fundamentals of Functionally Graded Materials*, London, UK, IOM Communications Limited (1998).
21. Santare, M.H. and Lambros, J. "Use of graded finite elements to model the behavior of nonhomogeneous materials", *ASME Journal of Applied Mechanics*, **67**, pp. 819-822 (2000).
22. Kim, J.H. and Paulino, G.H. "Isoperimetric graded finite elements for nonhomogeneous isotropic and orthotropic materials", *ASME Journal of Applied Mechanics*, **69**, pp. 502-514 (2002a).
23. Almajid, A. et al. "Analysis of out-of-plane displacement and stress field in a piezocomposite plate with functionally graded microstructure", *International Journal of Solids and Structures*, **38**, pp. 3377-3391 (2001).
24. Carbonari, R.C. et al. "Design of functionally graded piezoelectric actuators using topology optimization", in *Modeling, Signal Processing, and Control - 13th SPIE (Annual Symposium on Smart Structures and Materials)*, San Diego (2006).
25. Wazwaz, A. "A reliable algorithm for solving boundary value problems for higher-order integro-differential equations", *Appl. Math. Comput.*, **118**, pp. 327-342 (2001).
26. Hashim, I. "Adomian decomposition method for solving boundary value problems for fourth-order integro-differential equations", *J. Comput. Appl. Math.*, **193**, pp. 658-664 (2006).
27. Sadighi, A. et al. "Traveling wave solutions of the Sine-Gordon and the coupled Sine-Gordon equations using the homotopy-perturbation method", *Scientia Iranica, Transaction B*, **16**(2), pp. 189-195 (April 2009).
28. Adomian, G., *Nonlinear Stochastic Operator Equations*, Academic Press, Florida (1986).
29. Adomian, G. "Nonlinear stochastic systems theory and applications to physics", in *Mathematics and Its Applications*, **46**, Kluwer Academic Publishers Group, Dordrecht (1989).
30. Abdelwahid, F. "A mathematical model of Adomian polynomials", *Appl. Math. Comput.*, **141**(2-3), pp. 447-453 (2003).
31. Cherruault, Y. "Convergence of Adomian's method", *Mathematical and Computer Modelling*, **14**, pp. 83-86 (1990).

APPENDIX A

The expression of $\psi_{(s)}$ obtained using the Adomian decomposition method (up to 5th order term) is $\psi(s) = \sum_{n=1}^{12} \gamma_n \times s^{(n-1)}$ where:

$$\gamma_1 = 0,$$

$$\gamma_2 = c,$$

$$\gamma_3 = \frac{1}{2}\bar{K}_\lambda^2 \sin\alpha,$$

$$\gamma_4 = \frac{1}{6}c\bar{K}_\lambda^2 \cos\alpha,$$

$$\gamma_5 = \frac{\bar{K}_\lambda^2}{24}\left(\bar{K}_\lambda^2 \cos\alpha - c^2 \sin\alpha\right),$$

$$\gamma_6 = \frac{c\bar{K}_\lambda^2}{120}\left[\cos\alpha(\cos\alpha - c^2) - 3\bar{K}_\lambda^2 \sin\alpha\right],$$

$$\gamma_7 = \frac{\bar{K}_\lambda^2}{720}\left[c^4 \sin\alpha - c^2\bar{K}_\lambda^2(6\cos\alpha + 5\sin\alpha\cos\alpha)\right.$$
$$\left. - \bar{K}_\lambda^4(3\sin\alpha + \cos^2\alpha)\right],$$

$$\gamma_8 = \frac{c\bar{K}_\lambda^2}{5040}\left[\bar{K}_\lambda^2(\cos^2\alpha(\cos\alpha - 11c^2\bar{K}_\lambda^2)\right.$$
$$+ c^2\sin\alpha(10 + 5\sin\alpha) + c^4\cos\alpha)$$
$$\left. - 3\bar{K}_\lambda^4\cos\alpha(5 + 6\sin\alpha)\right],$$

$$\gamma_9 = \frac{\bar{K}_\lambda^4}{13440}\left\{3c^2\left[\bar{K}_\lambda^2(5\sin\alpha - 9\cos^2\alpha)\right.\right.$$
$$- \bar{K}_\lambda^2\sin\alpha(\frac{2}{7}\sin\alpha + 2\cos^2\alpha)$$
$$\left. + \frac{1}{3}c^2\cos\alpha(14\sin\alpha + \frac{560}{237})\right]$$
$$\left. - 2\bar{K}_\lambda^4\cos\alpha(15 + \cos^2\alpha)\right\},$$

$$\gamma_{10} = \frac{c\bar{K}_\lambda^2}{362880}\left\{\bar{K}_\lambda^6\left[3\sin\alpha(35+28\sin\alpha-27\cos^2\alpha)\right.\right.$$

$$\left.+\cos^2\alpha(\cos^2\alpha-225)\right]$$

$$+3c^2\left[\bar{K}_\lambda^2(c^2(19\cos^2\alpha-7\sin\alpha-14\sin^2\alpha)\right.$$

$$+5\bar{K}_\lambda^2\cos\alpha(7+5\sin^2\alpha))$$

$$\left.\left.-\cos\alpha(\bar{K}_\lambda^4(34\cos^2\alpha+162\sin\alpha)+(c^4/3))\right]\right\},$$

$$\gamma_{11} = \frac{\bar{K}_\lambda^4\sin\alpha}{3628800}\left[\bar{K}_\lambda^6(\cos^4\alpha+189\sin^4\alpha\right.$$

$$-306\sin^2\alpha\cos^2\alpha)$$

$$-3c^4\bar{K}_\lambda^2(327\sin^2\alpha+641\cos^2\alpha)-247c^6\cos\alpha$$

$$\left.+2c^2\bar{K}_\lambda^4\cos\alpha(1683\sin^2\alpha-461\cos^2\alpha)\right],$$

$$\gamma_{12} = \frac{c\bar{K}_\lambda^6}{39916800}\left\{\bar{K}_\lambda^4(\cos^5\alpha-2766\cos^3\alpha\sin^2\alpha\right.$$

$$+8289\cos\alpha\sin^4\alpha+3c^4(641\cos^3\alpha$$

$$-2757\cos\alpha\sin^2\alpha)-c^2\bar{K}_\lambda^4\left[810(9\sin^4\alpha\right.$$

$$\left.\left.-1142\sin^2\alpha\cos^2\alpha)+922\cos^4\alpha\right]\right\}.$$